Environ Geol (2007) 52:11–18
DOI 10.1007/s00254-006-0444-5

ORIGINAL ARTICLE

Study of galvanic interactions between pyrite and chalcopyrite in a flowing system: implications for the environment

Liu Qing You · Li Heping · Zhou Li

Received: 14 March 2006 / Accepted: 11 July 2006 / Published online: 15 August 2006

Abstract When galvanic interactions between pyrite and chalcopyrite occur in solution, pyrite, with the higher rest potential, acts as a cathode and is protected whereas chalcopyrite, with the lower rest potential, acts as an anode and its oxidation is increased. In this work a three-electrode system was used to investigate the corrosion current density and mixed potential of a galvanic cell comprising a pyrite cathode and a chalcopyrite anode in a flowing system. The results showed that with increasing concentration of ferric ion in the solution, with increasing acidity, and with increasing flow rate of the solution, the corrosion current density increased and the mixed potential of the galvanic cell became more positive. These experimental results are of direct significance to the control of environmental pollution in mining activity. By using the galvanic model, mixed potential theory, and the Butler–Volmer equation, the experimental results were explained theoretically.

Keywords Pyrite · Chalcopyrite · Galvanic interaction · Flowing system · Environmental pollution

L. Qing You · L. Heping (✉) · Z. Li
Laboratory for Study of the Earth's Interior and Geofluids, Institute of Geochemistry, Chinese Academy of Sciences, Guiyang 550002, China
e-mail: liheping@vip.gyig.ac.cn

L. Qing You · Z. Li
Graduate School, Chinese Academy of Sciences, Beijing 100039, China

Introduction

In nature, most metal sulfide minerals have the properties of a semiconductor. Because of the narrow energy band structure of sulfide minerals, dissolution of the mineral can be regarded as the corrosion process of a galvanic cell. The mineral, or the region, with the highest rest potential will act as the cathode of the galvanic cell and be protected whereas that with the lowest rest potential will serve as anode, and its rate of dissolution will be increased (Nicol 1975; Mehta and Murr 1982; Natarajan and Iwasaki 1983; Woods 2000; Mahmood and Turner 1985; Palencia et al. 1991).

Pyrite and chalcopyrite, the most common and exploitable sulfide minerals, usually occur together and in contact with each other. In the past, research on the galvanic interactions between pyrite and chalcopyrite mainly focussed on hydrometallurgy. Majima and Peter (1968) pointed out that galvanic effect might be one of the most important electrochemical factors governing the rate of dissolution of sulfide minerals in hydrometallurgical systems. Mehta and Murr (1983) experimentally studied the galvanic interactions between a series of sulfide minerals, including the pyrite–chalcopyrite couple. The experimental results revealed that the galvanic interactions between pyrite and chalcopyrite significantly affected leaching and extraction of chalcopyrite from a mixed-ore slurry of pyrite and chalcopyrite. The presence of pyrite in the slurry led to a 2–15 times increase in the rate of dissolution of chalcopyrite. Ekmekçi and Demirel (1997) studied the effects of galvanic interactions between pyrite and chalcopyrite during flotation without a collector. They found that galvanic interactions between pyrite and chalcopyrite significantly affected

the flotation behaviour of the two minerals, i.e. flotation of the pyrite was promoted whereas that of chalcopyrite was hampered to some extent.

Galvanic interactions between pyrite and chalcopyrite also have a large effect on geochemical processes (Li 1995). Sikka et al. (1991) examined secondary copper ore samples from the Malanjkhand porphyry copper deposit of India and found that chalcopyrite was gradually altered into sulfur-poor and Cu-rich secondary sulfide minerals in the order: chalcopyrite ($CuFeS_2$)–bornite (Cu_5FeS_4)–idaite (Cu_3FeS_4)–covellite (CuS)–yarrowite (Cu_9S_8)–spionkopite ($Cu_{39}S_{28}$)–geerite ($Cu_{1.60}S$)–anilite ($Cu_{1.75}S$)–djurleite ($Cu_{1.943}S$)–chalcocite (Cu_2S). They pointed out that the alteration of chalcopyrite is mainly the result of galvanic interactions. Probable and possible stability relationships among different phases are suggested in terms of Eh–Ph and attendant galvanic reactions in oxygenated and carbonated waters percolating through the rock and ore body. Several electrochemical equations are proposed for the reactions and stability fields of the minerals have been derived by use of available thermodynamic data.

With the development of the mining and metallurgical industries and with increased awareness of the need for environmental protection, environmental issues in mining and mineral processing activities are currently attracting increasing attention. The high dissolved metal content of acidic mine drainage generated from mining and mineral processing activities can pass into surface and ground water and cause a variety of environmental problems, for example water and soil pollution, resulting in great damage to human health and a devastating effect on terrestrial and aquatic ecosystems (Zhang et al. 2004a, b; Liu et al. 2002). More serious, the different sources of pollution will remain for a very long time, even when all the activity has ceased (Benvenuti et al. 1997). Oxidative dissolution of metal sulfides by the galvanic interaction mechanism is an important factor leading to environmental pollution in metal sulfide mine areas (Byerley and Scharer 1992; Lin 1997; Dinelli and Tateo 2002; Salomons 1995; Subrahmanyam and Forssberg 1993; Cruz et al. 2001).

As far as we are aware, no data have yet been reported on galvanic interactions between pyrite and chalcopyrite in a flowing system. Previous reports have shown:

1. in a metal sulfide mine, the mine drainage usually contains Fe^{3+} at different concentrations, and its pH ranges from 2 to 4 (Elliott et al. 1998);
2. the pH ofacid rainwater is <5.6; and
3. the flow rate of mountainous brooks is usually greater than 0.3 m s^{-1} (Merkblatt 2000).

In this work we investigated the galvanic interactions between pyrite and chalcopyrite in solutions with broader ranges of pH, Fe^{3+} concentration, and flow rate than mine drainage and acidic rainwater in an attempt to:

– clarify the mechanism of the galvanic interactions between pyrite and chalcopyrite in flowing solutions;
– determine the dependence of heavy metal pollution on the features of the flowing media (pH, Fe^{3+} concentration, and flow rate); and, ultimately,
– provide the theoretical basis for environmental protection and harness of metal sulfide mine areas.

Experimental methods

Pyrite and chalcopyrite used in the experiments were collected from the Dongquan copper deposit of Yunnan Province, China, and their electron microprobe analysis results are presented in Table 1.

The crude samples were first ground into 8 mm diameter cylinders and a copper wire was soldered on to one end surface of each cylinder. The cylinders were the put into appropriately sized Teflon tubes, followed by injection of epoxy resin for sealing and fixing. Metallographic abrasive papers of grades $1^{\#}$–$5^{\#}$ were used to polish the other end surface of each cylinder, i.e. the working surface of the electrodes. Only the working surface of the electrode was in contact with the solution during experiments. The polished electrodes were all composed of pure pyrite or chalcopyrite, as observed under a reflecting microscope. Before each use of the electrodes, the working surfaces of the electrodes were polished with metallographic paper, to expose fresh surfaces, and then washed with acetone and distilled water until the surfaces were sufficiently clean.

A three-electrode system was adopted in the experiments. An HP-34401A high-precision digital

Table 1 Chemical composition of pyrite and chalcopyrite samples (%, *w*/*w*)

Element	$CuFeS_2$	FeS_2
Cu	34.54	–
Fe	30.70	46.89
Ni	–	0.0015
S	34.67	52.96

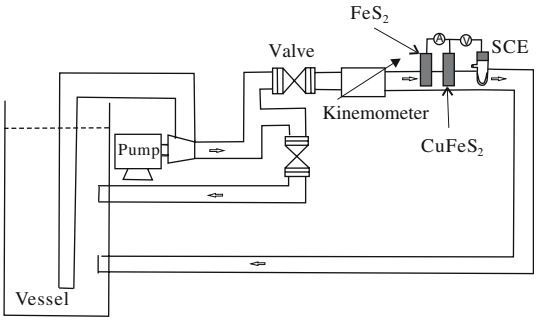

Fig. 1 Schematic drawing of the experimental arrangement

multimeter, connected to a computer, was used to measure the corrosion current density and mixed potential. A saturated calomel electrode was used as the reference electrode. The experimental arrangement is shown schematically in Fig. 1.

Results and discussion

To measure the effects of Fe^{3+} concentration, solution acidity, and solution flow rate on the galvanic interactions, we performed a series of experiments. Detailed experimental conditions are given in Table 2.

Figure 2 depicts the variation of corrosion current density and mixed potential for different Fe^{3+} concentrations. It is apparent that when the solution contains Fe^{3+} the corrosion current density of the pyrite–chalcopyrite couple tends to increase substantially; the greater the concentrations of Fe^{3+}, the higher the corrosion current density and the longer it takes to reach equilibrium. The mixed potential becomes more positive with increasing concentrations of Fe^{3+}.

Figure 3 depicts the variation of corrosion current density and mixed potential for simulated rainwater of different pH. It is clearly apparent from Fig. 3 that the lower the pH of the solution, i.e. the greater the acidity, the greater the corrosion current density and the more positive the mixed potential.

Figure 4 depicts the variation of corrosion current density and mixed potential for simulated mine-discharge water at different flow rates. It is apparent from Fig. 4 that with increasing flow rate of the solution the corrosion current density increases substantially and the mixed potential becomes much more positive.

According to the previous reports (Dutrizac and MacDonald 1973; Munoz et al 1979; Dutrizac 1981; Hackl et al. 1995; Hiroyoshi et al. 2002; Lu et al. 2000a, b), when galvanic interactions between pyrite and chalcopyrite occur under acidic conditions the chalcopyrite acts as the anode and the oxidation reaction occurs on its surface:

$$CuFeS_2 \rightarrow Cu^{2+} + Fe^{2+} + 2S^0 + 4e. \quad (1)$$

whereas pyrite acts as the cathode and reduction reactions occur on its surface:

$$O_2 + 4H^+ + 4e \rightarrow 2H_2O \quad (2)$$

$$Fe^{3+} + e \rightarrow Fe^{2+}. \quad (3)$$

The overall galvanic reaction can be expressed as:

$$CuFeS_2 + O_2 + 4H^+ \rightarrow Cu^{2+} + Fe^{2+} + 2S^0 + 2H_2O \quad (4)$$

$$CuFeS_2 + 4Fe^{3+} \rightarrow Cu^{2+} + 5Fe^{2+} + 2S^0. \quad (5)$$

During the galvanic interactions, electrons are lost from $CuFeS_2$ and transferred from $CuFeS_2$ to FeS_2, and the oxidation reaction (Eq. 1) and the reduction reactions (Eqs. 2 and 3) above occur on the surfaces of $CuFeS_2$ and FeS_2, respectively. The mechanism of pyrite–chalcopyrite galvanic interactions is shown in Fig. 5.

But, because the solubility of O_2 is very low (8–8.5 mg L^{-1}) at room temperature and, therefore,

Table 2 Detailed experimental conditions

Experimental number	Different Fe^{3+} concentrations (Fig. 2)	Different solution acidity (Fig. 3)	Different flow rates (Fig. 4)
1	0.36 ms^{-1}, 0 mol L^{-1}	0.36 ms^{-1}, pH 6.97	$n_{Fe^{3+}} = 0.01$ mol L^{-1}, pH 3.78, 0.06 ms^{-1}
2	0.36 ms^{-1}, 0.0001 mol L^{-1}	0.36 ms^{-1}, pH 5.97	$n_{Fe^{3+}} = 0.01$ mol L^{-1}, pH 3.78, 0.24 ms^{-1}
3	0.36 ms^{-1}, 0.001 mol L^{-1}	0.36 ms^{-1}, pH 4.97	$n_{Fe^{3+}} = 0.01$ mol L^{-1}, pH 3.78, 0.36 ms^{-1}
4	0.36 ms^{-1}, 0.01 mol L^{-1}	–	–

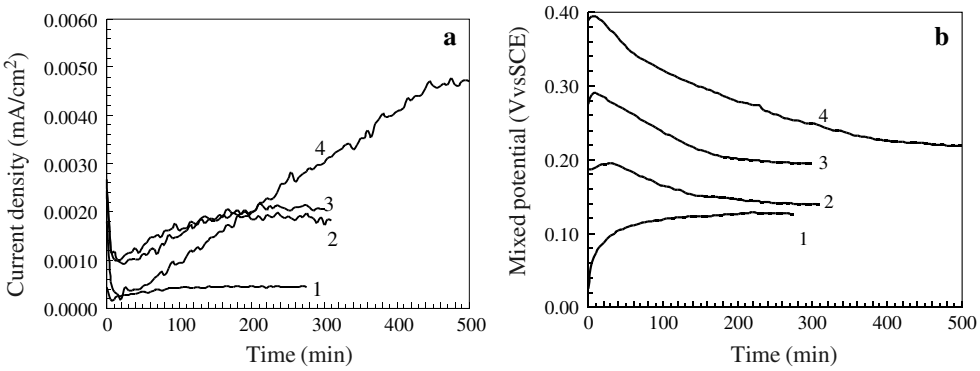

Fig. 2 Variation of corrosion current density (**a**) and mixed potential (**b**) for different ferric ion concentrations (25°C, flow rate 0.36 ms^{-1}, (*1*) $n_{Fe^{3+}} = 0\,mol\,L^{-1}$; (*2*) $n_{Fe^{3+}} = 0.0001\,mol\,L^{-1}$; (*3*) $n_{Fe^{3+}} = 0.001\,mol\,L^{-1}$; (*4*) $n_{Fe^{3+}} = 0.01\,mol\,L^{-1}$)

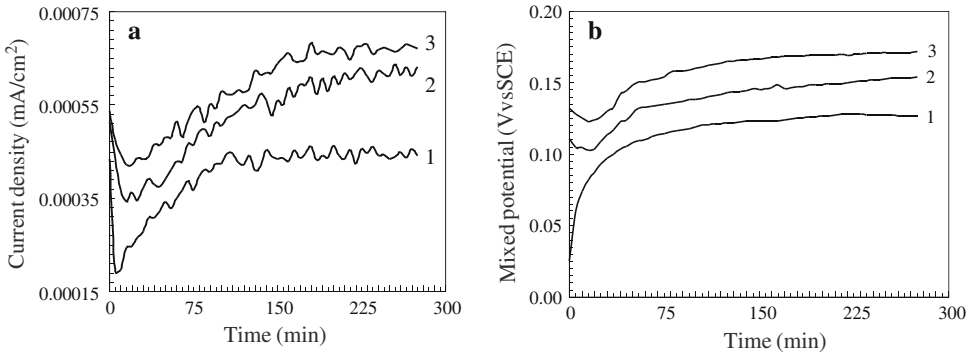

Fig. 3 Variation of corrosion current density (**a**) and mixed potential (**b**) at different acidity (25°C, flow rate 0.36 ms^{-1}, (*1*) pH 6.97; (*2*) pH 5.97; (*3*) pH 4.97)

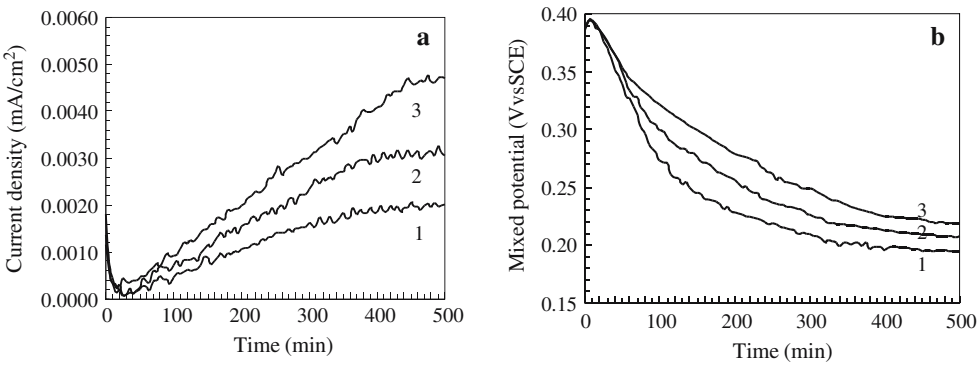

Fig. 4 Variations of corrosion current density (**a**) and mixed potential (**b**) at different flow rates (25°C, $n_{Fe^{3+}} = 0.01\,mol\,L^{-1}$, pH 3.78, (*1*) flow rate 0.06 ms^{-1}; (*2*) flow rate 0.24 ms^{-1}; (*3*) flow rate 0.36 ms^{-1})

the limiting current density of the cathode and the corrosion current density of the galvanic cell will be very small (Hu 1991), the presence of Fe^{3+} will dominate the galvanic interactions, owing to its strong oxidizability and the effect of dissolved oxygen on galvanic corrosion can be neglected. The Butler–Volmer equations for the reactions depicted by Eqs. 1 and 3 are presented below (Hu 1991; Cao 1985):

$$\begin{aligned} i_a = i_{CuFeS_2} &= i^0_{CuFeS_2}\left[\exp\frac{\alpha_{CuFeS_2}}{RT}\eta_a - \exp\left(-\frac{(1-\alpha_{CuFeS_2})}{RT}\eta_c\right)\right] \\ &= i^0_{CuFeS_2}\left[\exp\frac{\alpha_{CuFeS_2}}{RT}(E_g - E_{e,CuFeS_2}) - \exp\left(-\frac{(1-\alpha_{CuFeS_2})}{RT}(E_g - E_{e,CuFeS_2})\right)\right] \end{aligned} \quad (6)$$

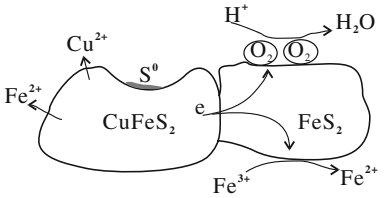

Fig. 5 Schematic diagram of pyrite–chalcopyrite galvanic interactions

$$i_c = i_{Fe^{3+}} = i^0_{Fe^{3+}}\left[\exp\frac{\alpha_{Fe^{3+}}F}{RT}\eta_c - \exp\left(-\frac{(1-\alpha_{Fe^{3+}})F}{RT}\eta_c\right)\right] = i^0_{Fe^{3+}}\left[\exp\frac{\alpha_{Fe^{3+}}F}{RT}(E_{e,Fe^{3+}} - E_g) - \exp\left(-\frac{(1-\alpha_{Fe^{3+}})F}{RT}(E_{e,Fe^{3+}} - E_g)\right)\right] \quad (7)$$

where i_a and i_c are the current densities of the anode and cathode, respectively; $i^0_{CuFeS_2}, i^0_{Fe^{3+}}$ are the exchange current densities of $CuFeS_2$ anode reaction and Fe^{3+}/Fe^{2+} cathode reaction, respectively; E_g is the mixed potential (corrosion potential) of the galvanic cell; $E_{e,CuFeS_2}, E_{e,Fe^{3+}}$ are the equilibrium potentials of the anode and cathode, respectively; $\alpha_{CuFeS_2}, \alpha_{Fe^{3+}}$ are the transfer coefficients of the anode and cathode; respectively; R is the gas constant; F is the Faraday constant; and T is the absolute temperature.

Because the corrosion galvanic interaction is a spontaneous oxidation–reduction process, it follows that $E_{e,a} < E_g < E_{e,c}$ must be true. In our experiments, the corrosion potential E_g deviated far from the anode equilibrium potential $E_{e,CuFeS_2}$ and the cathode equilibrium potential $E_{e,Fe^{3+}}$. Anode oxidation and cathode reduction are, therefore, both of strong polarization and the inverse processes of electrode reactions can be neglected. Equations 6 and 7 can be simplified as:

$$i_a = i_{CuFeS_2} = i^0_{CuFeS_2}\exp\frac{\alpha_{CuFeS_2}F}{RT}(E_g - E_{e,CuFeS_2}) \quad (8)$$

and

$$i_c = i_{Fe^{3+}} = i^0_{Fe^{3+}}\exp\frac{\alpha_{Fe^{3+}}F}{RT}(E_{e,Fe^{3+}} - E_g). \quad (9)$$

According to the mixed potential theory, at the mixed potential E_g, cathode current density i_c and anode current density i_a are equal to the current density of the galvanic reaction i_g.

$$i_a = -i_c = i_g. \quad (10)$$

Substituting Eqs. 8 and 9 into Eq. 10, we obtain the equations:

$$E_g = \frac{\beta_a\beta_c}{\beta_a+\beta_c}\ln\frac{i^0_{Fe^{3+}}}{i^0_{CuFeS_2}} + \frac{\beta_a}{\beta_a+\beta_c}E_{e,Fe^{3+}} + \frac{\beta_a}{\beta_a+\beta_c}E_{e,CuFeS_2} \quad (11)$$

and

$$i_g = \left(i^0_{CuFeS_2}\right)^{\beta_a/(\beta_a+\beta_c)}\left(i^0_{Fe^{3+}}\right)^{\beta_a/(\beta_a+\beta_c)} \times \exp\left(\frac{E_{e,Fe^{3+}} - E_{e,CuFeS_2}}{\beta_a+\beta_c}\right) \quad (12)$$

where $\beta_a = RT/\alpha_{CuFeS_2}F, \beta_c = RT/\alpha_{Fe^{3+}}F$.

Holmes and Crundwell (1995) pointed out that an increase in the concentration of ferric ions results in an increase in the electrode potentials and equilibrium potentials of both cathode and anode; it will also change the dynamics for both half-reactions and increase the exchange current densities. Equation 11 indicates that an increase in the concentration of ferric ions results in an increase in the mixed potential. This theoretical result is highly consistent with the experimental result shown in Fig. 2b.

The driving force of the galvanic reaction is the difference between $E_{e,Fe^{3+}}$ and $E_{e,CuFeS_2}$, i.e. $E_{e,Fe} - E_{e,CuFeS_2}$. From the paragraph above we know that increases the concentration of ferric ions makes the mixed potential more positive. The more positive potential is of advantage to the reduction of Fe^{3+} more than the oxidation of $CuFeS_2$, thus making the driving force $E_{e,Fe} - E_{e,CuFeS_2}$ become larger. From Eq. 11 we can see that when the concentrations of Fe^{3+} in the solution are enhanced, the corrosion current density of galvanic cells made of pyrite and chalcopyrite will increase, consistent with the experimental results shown in Fig. 2a.

Shown in Fig. 6 is the i–E variation curve for the mixed potential model, at different Fe^{3+} concentrations, for the pyrite–chalcopyrite galvanic cell. The results reveal the effect of the increase in Fe^{3+} con-

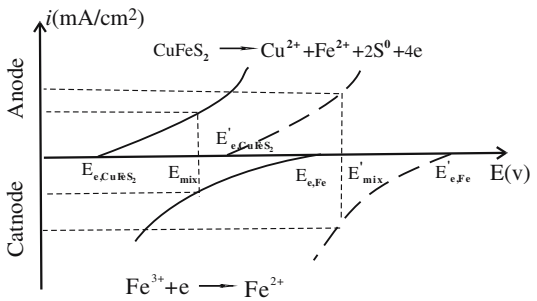

Fig. 6 i–E variation curve for the mixed potential model at different Fe^{3+} concentrations

centrations on the mixed potential and corrosion current density of the pyrite–chalcopyrite galvanic cell. The dashed lines indicate the *i–E* variation curves for the corresponding anode and cathode when the concentration of Fe^{3+} in the solution increases.

In solutions without Fe^{3+} the galvanic reactions at the anode and cathode are oxidation of chalcopyrite (Eq. 1) and reduction of O_2 (Eq. 2), respectively. Similar to the discussion above, we can obtain:

$$E_g = \frac{\beta_a \beta_c}{\beta_a + \beta_c} \ln \frac{i^0_{O_2}}{i^0_{CuFeS_2}} + \frac{\beta_a}{\beta_a + \beta_c} E_{e,O_2} + \frac{\beta_a}{\beta_a + \beta_c} E_{e,CuFeS_2} \tag{13}$$

and

$$i_g = \left(i^0_{CuFeS_2}\right)^{\frac{\beta_a}{\beta_a+\beta_c}} \left(i^0_{O_2}\right)^{\frac{\beta_c}{\beta_a+\beta_c}} \exp\left(\frac{E_{e,O_2} - E_{e,CuFeS_2}}{\beta_a + \beta_c}\right) \tag{14}$$

where $\beta_a = RT/\alpha_{CuFeS_2}F, \beta_c = RT/\alpha_{O_2}F$.

Many studies (e.g. Abramov 1965; Abramov et al. 1975) have shown that the electrode potential of a mineral in a solution depends on the intrinsic properties of the mineral, the acidity of the solution, and the concentration of dissolved oxygen in the solution. According to Rao and Finch (1988) and Majima (1969):

1. if the acidity of the solution increases, the equilibrium electrode potentials of both pyrite and chalcopyrite will become more positive; and
2. increasing the concentration of H^+ in the solution will lead to an increase in the exchange current density of both cathode and anode, i.e., $i^0_{O_2}$ and $i^0_{CuFeS_2}$.

From Eq. 13, therefore, we can see that the increase in the concentration of H^+ in the solution will lead to enhancement of the mixed potential of the pyrite–chalcopyrite galvanic cell, in accordance with the experimental results shown in Fig. 3b.

Moreover, as for the Fe^{3+}-bearing solutions, because the mixed potential of the galvanic cell becomes more positive, it has a greater effect on reduction of O_2 than on oxidation of $CuFeS_2$, thus increasing the driving force $E_{e,O_2} - E_{e,CuFeS_2}$ of the pyrite–chalcopyrite galvanic cell in solutions without Fe^{3+}. According to Eq. 14, increasing the concentration of H^+ in solutions without Fe^{3+} can enhance the corrosion current density of the pyrite–chalcopyrite galvanic cell; this is consistent with the experimental results shown in Fig. 3a.

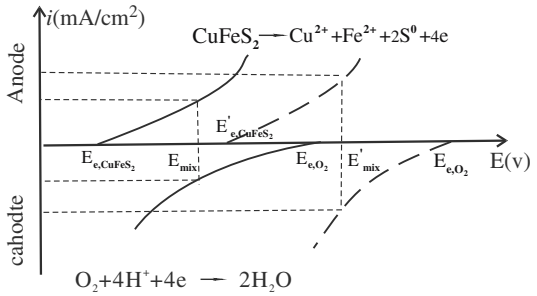

Fig. 7 *i–E* variation curves of the mixed potential model for solutions of different acidity

According to the mixed potential theory, the *i–E* variation curves for the pyrite–chalcopyrite galvanic cell in solutions of different acidity without Fe^{3+} can be established as shown in Fig. 7, with the dashed lines indicating the *i–E* curves for the corresponding cathode and anode electrodes. The curves in Fig. 7 also show that variation of the mixed potential and the corrosion current density of the galvanic cell with solution acidity is the same as was obtained in our experiments.

According to Zha et al. (2002), the current density expression on the electrode surface is:

$$i = \frac{nFD_i}{v_i} \frac{c_i^0 - c_i^s}{\delta_i} \tag{15}$$

where v_i, D_i and δ_i are, respectively, the reaction coefficient, diffusion coefficient, and diffusion layer thickness of ion i; c_i^0 and c_i^s are the concentrations of ion i in the bulk solution and on the electrode surface, respectively, and n and F are the electron transfer number and Faraday constant, respectively. Under flowing aqueous solution conditions, the diffusion layer thickness δ_i can be expressed as:

$$\delta_i = D_i^{1/3} \gamma^{1/6} y^{1/2} u_0^{-1/2} \tag{16}$$

where γ is the dynamic viscosity coefficient, y is the distance from a particular point to the impact point y_0, and u_0 is the flow rate of solution.

From Eq. 16 it is apparent that the diffusion layer thickness δ_i is in direct proportion to $u_0^{-1/2}$, and if the flow rate of the solution is increased the diffusion layer thickness δ_i will become thinner. As a result, the thinner the diffusion layer thickness δ_i, the larger the corrosion current density is, in accordance with Eq. 15;

this is consistent with the experimental results shown in Fig. 4a. On the other hand, when the flow rate of the solution increases, the products on the electrode surface will be easily carried away; at the same time the reactants will be brought more rapidly to the electrode surface, leading to intensification of depolarization, thus making the mixed potential more positive, also in agreement with the experimental results shown in Fig. 4b.

Environmental implications

The results of this study indicate:

1. Solution flow can increase the speed of galvanic interactions. So, the higher the flow rates of mine-discharge water and rain water, the higher the amounts of heavy metals and acids produced in unit time and, therefore, the more serious the environmental pollution in the mining districts and surrounding areas.
2. When pyrite is in contact with chalcopyrite in solution, pyrite is protected and chalcopyrite is preferentially dissolved. When this system occurs in nature, therefore, the chemical components of chalcopyrite will be released first and the pyrite will be galvanically protected by adjacent chalcopyrite until all the chalcopyrite has disappeared.
3. Because Fe^{3+} in the flowing solution can increase the speed of galvanic interactions, galvanic interactions cannot be prevented merely by excluding oxygen. When abandoned mines and ore tailings or mining wastes contain a variety of sulfide minerals, it seems unlikely that building in-situ sub-surface hydrologic barriers in the mining field, as proposed by Waring and Tayler (1999), will improve the acidic waste water discharged or heavy metal pollution.

By making use of the corrosion galvanic interactions principle Shelp et al. (1995, 1996) studied how to use electrochemical technology to ameliorate acid mine drainage problems occurring at the Sherman Iron Ore Mine of Temagami, Ontario, Canada. A series of laboratory experiments were conducted using a block of massive sulfide rock from the mine site as the cathode, scrap iron, Al, and Zn as the sacrificial anodes, and acidic leachate collected from the mine site as the electrolyte. Their study showed it was possible to generate sufficient voltage and current to increase the pH of acid leachate, to maintain it at an environmentally acceptable level of 5.6, and to significantly reduce the redox potential, thus inhibiting oxidation of sulfide minerals. Another advantage was that potentially toxic elements, for example Al, Cd, Co, Cu, and Ni, and other trace elements, could be scavenged from solution by formation of a relatively stable Fe/Al sulfate precipitate. Study of corrosion galvanic interactions may therefore provide clues and a scientific basis for controlling mine pollution caused by metal sulfides.

Conclusions

1. When the solution contains Fe^{3+}, the corrosion current density of galvanic interactions between pyrite and chalcopyrite increases; the higher the concentration of Fe^{3+}, the greater the corrosion current density and the more positive the mixed potential. Effectively reducing the concentration of Fe^{3+} and other strongly oxidizing species in flowing solutions might be an important means of improving the environment in metal sulfide mining areas.
2. The greater the acidity of the solution, the higher the corrosion current density and the more positive the mixed potential of the galvanic cell. Therefore, effectively reducing the concentration of H^+ in flowing solutions might be another important means of controlling environmental pollution in metal sulfide mining areas.
3. For solutions with given concentrations of components and acidity, the greater the flow rate of the solutions the higher the corrosion current density and the more positive the mixed potential of the galvanic cell. Flow of different surface and underground water through pyrite and chalcopyrite that are in contact can therefore increase the speed of reactions of the galvanic cell between pyrite and chalcopyrite, leading to more serious deterioration of the environment in metal sulfide mining areas.

Acknowledgements This research was supported by a grant from the Knowledge–Innovation Program sponsored by the Chinese Academy of Sciences (KZCX3-SW-124). Senior Engineer Wang Mingzai of the Institute of Geochemistry, Chinese Academy of Sciences, conducted the electron microprobe analysis on samples. We are indebted to Senior Engineers Xu Huigang and Yang Meiqi for their helpful instructions in our experiments.

References

Abramov AA (1965) Effect of pH on the condition of the pyrite surface. Tsvetn Met 6(12):33–36

Abramov AA, Abdokhin UM, Dzugkoeva EM, Korzhova RV, Safin KS (1975) Surface conditions of minerals under flotation. Tsvetn Met 16(3):92–96

Benvenuti M, Mascaro I, Corsini F (1997) Mine waste dumps and heavy metal pollution in abandoned mining district of Boccheggiano (Southern Tuscany, Italy). Environ Geol 30(3–4):238–243

Byerley JJ, Scharer JM (1992) Natural release of copper and zinc into the aquatic environment. Hydrometallurgy 30(1–3): 107–126

Cao C (1985) Principles of corrosion electrochemistry. Chemical Industrial Publishing House, Beijing, pp 102–110

Cruz R, Bertrand V, Monroy M, González I (2001) Effect of sulfide impurities on the reactivity of pyrite and pyritic concentrates: a multi-tool approach. Appl Geochem 16(7–8):803–819

Dinelli ED, Tateo F (2002) Different types of fine-grained sediments associated with acid mine drainage in the Libiola Fe–Cu mine area (Ligurian Apennines, Italy). Appl Geochem 17(8):1081–1092

Dutrizac JE (1981) The dissolution of chalcopyrite in ferric sulfate and ferric chloride media. Metall Trans B 12:371–378

Dutrizac JE, MacDonald RJC (1973) The effect of some impurities on the rate of chalcopyrite dissolution. Can Metall Q 12(4):409–420

Ekmekçi Z, Demirel H (1997) Effects of galvanic interaction on collectorless flotation behaviour of chalcopyrite and pyrite. Int J Miner Process 52(1):31–48

Elliott P, Ragusa S, Catcheside D (1998) Growth of sulfate-reducing bacteria under acidic conditions in an upflow anaerobic bioreactor as a treatment system for acid mine drainage. Water Res 32(12):3724–3730

Hackl RP, Dreisinger DB, Peters E, King JA (1995) Passivation of chalcopyrite during oxidative leaching in sulfate media. Hydrometallurgy 39(1–3):25–48

Hiroyoshi N, Arai M, Miki H, Tsunekawa M, Hirajima T (2002) A new reaction model for the catalytic effect of silver ions on chalcopyrite leaching in sulfuric acid solutions. Hydrometallurgy 63(3):257–267

Holmes PR, Crundwell FK (1995) Kinetic aspects of galvanic interactions between minerals during dissolution. Hydrometallurgy 39(1–3):353–375

Hu M (1991) Corrosion electrochemistry. Metallurgical Industrial Publishing House, Beijing, pp 181–236

Li HP (1995) Natural primary cells geochemistry. PhD Thesis, Department of Geology, Central South University of Technology, Changsha, China

Lin ZX (1997) Mobilization and retention of heavy metals in mill-tailings from Garpenberg sulfide mines, Sweden. Sci Total Environ 198(1):13–31

Liu CQ, Wu JH and Yu WH (2002) Interactions at iron hydroxide colloid/water interface and REE fractionations in surface waters: experimental study on pH-controlling mechanism. Sci China (Ser D) 45:449–458

Lu ZY, Jeffrey MI, Lawson F (2000a) An electrochemical study of the effect of chloride ions on the dissolution of chalcopyrite in acidic solutions. Hydrometallurgy 56(2):145–155

Lu ZY, Jeffrey MI, Lawson F (2000b) The effect of chloride ions on the dissolution of chalcopyrite in acidic solutions. Hydrometallurgy 56(2):189–202

Mahmood MN, Turner AK (1985) The selective leaching of zinc from chalcopyrite–sphalerite concentrates using slurry electrodes. Hydrometallurgy 14(3):317–329

Majima H (1969) How oxidation affects selective flotation of complex sulfide ores. Can Metall Q 8:269–273

Majima H, Peter E (1968) Electrochemistry of sulfide dissolution in hydrometallurgical systems. In: Proc Int Proc Cong, Leningrad, 13 pp

Mehta AP, Murr LE (1982) Kinetic study of sulfide leaching by galvanic interaction between chalcopyrite, pyrite and sphalerite in the presence of *T. ferroxidans* and thermophilic micro-organism. Biotech Bioeng 24:919–940

Mehta AP, Murr LE (1983) Fundamental studies of the contribution of galvanic interaction to acid-bacterial leaching of mixed metal sulfides. Hydrometallurgy 9(3):235–256

Merkblatt ATV (2000) DVWK M 153 Handlungsempfehlungen zum Umgang mit Regenwasser. GFA Gesellschaft zur Förderung der Abwassertechnik e.V., Hennef

Munoz PB, Miller JD, Wadsworth ME (1979) Reaction mechanism for the acid ferric leaching of chalcopyrite. Metall Trans B 10:149–158

Natarajan KA, Iwasaki I (1983) Role of galvanic interactions in the bioleaching of Duluth gabbro copper-nickel sulfides. Sep Sci Technol 18:1095–1111

Nicol MJ (1975) Mechanism of aqueous reduction of chalcopyrite by copper, iron, and lead. Trans Min Metall 84:206

Palencia I, Wan RY, Miller JD (1991) The electrochemical behavior of a semiconducting natural pyrite in the presence of bacteria. Metall Trans B 24:717–727

Rao SR, Finch JA (1988) Galvanic interaction studies on sulfide minerals. Can Metall Q 27:253–259

Salomons W (1995) Environmental impact of metals derived from mining activities: processes, predictions, prevention. J Geochem Explor 52(1–2):5–23

Shelp GS, Chesworth W, Spiers G (1995) The amelioration of acid mine drainage by an in situ electrochemical method—I. Employing scrap iron as the sacrificial anode. Appl Geochem 10(6):705–713

Shelp GS, Chesworth W, Spiers G (1996) The amelioration of acid mine drainage by an in situ electrochemical method; part 2: employing aluminium and zinc as sacrificial anodes. Appl Geochem 11(3):425–432

Sikka DB, Petruk W, Nehru CE, Zhang Z (1991) Geochemistry of secondary copper minerals from Proterozoic porphyry copper deposit, Malanjkhand, India. Ore Geol Rev 6(2–3):257–290

Subrahmanyam TV, Forssberg KS (1993) Mineral solution-interface chemistry in minerals engineering. Miner Eng 6(5):439–454

Waring CL, Taylor JR (1999) A new technique for building in situ sub-surface hydrologic barriers: NBT. In: Int Mine Water Assoc (IMWA) Conf, Seville, Spain, pp 663–666

Woods R (2000) Recent advances in electrochemistry of sulfide mineral flotation. Trans Nonferrous Met Soc China 10:26–29

Zha Q (2002) Introduction to dynamics of electrode processes, 3rd edn. Science Press, Beijing, pp 84–88

Zhang G, Liu CQ, Yang Y, Wu P (2004a) The characteristics of heavy metals and sulfur isotope of water draining lead–zinc mine in carbonate area. Water Air Soil Pollut 155:51–62

Zhang G, Liu CQ, Wu P, Yang Y (2004b) The geochemical characteristics of mine-waste calcines and runoff from the Wanshan mercury mine, Guizhou, China. Appl Geochem 19(11):1735–1744